Author Manuscript

Author Manuscript

Author Manuscript

Author Manuscript

HHS Public Access

Author manuscript

Cell Rep. Author manuscript; available in PMC 2019 April 12.

Published in final edited form as:

Cell Rep. 2019 April 02; 27(1): 226–237.e4. doi:10.1016/j.celrep.2019.03.029.

HIF-1α Is a Metabolic Switch between Glycolytic-Driven Migration and Oxidative Phosphorylation-Driven Immunosuppression of Tregs in Glioblastoma

Jason Miska[1], **Catalina Lee-Chang**[1], **Aida Rashidi**[1], **Megan E. Muroski**[1], **Alan L. Chang**[1], **Aurora Lopez-Rosas**[1], **Peng Zhang**[1], **Wojciech K. Panek**[1], **Alex Cordero**[1], **Yu Han**[1], **Atique U. Ahmed**[1], **Navdeep S. Chandel**[2], and **Maciej S. Lesniak**[1,3,*]

[1]Department of Neurological Surgery, Feinberg School of Medicine, Northwestern University, 676 North St. Clair Street, Suite 2210, Chicago, IL 60611, USA

[2]Department of Medicine, Feinberg School of Medicine, Northwestern University, 676 North St. Clair Street, Suite 2330, Chicago, IL 60611, USA

[3]Lead Contact

SUMMARY

The mechanisms by which regulatory T cells (Tregs) migrate to and function within the hypoxic tumor microenvironment are unclear. Our studies indicate that specific ablation of hypoxia-inducible factor 1α (HIF-1α) in Tregs results in enhanced $CD8^+$ T cell suppression versus wild-type Tregs under hypoxia, due to increased pyruvate import into the mitochondria. Importantly, HIF-1α-deficient Tregs are minimally affected by the inhibition of lipid oxidation, a fuel that is critical for Treg metabolism in tumors. Under hypoxia, HIF-1α directs glucose away from mitochondria, leaving Tregs dependent on fatty acids for mitochondrial metabolism within the hypoxic tumor. Indeed, inhibition of lipid oxidation enhances the survival of mice with glioma. Interestingly, HIF-1α-deficient-Treg mice exhibit significantly enhanced animal survival in a murine model of glioma, due to their stymied migratory capacity, explaining their reduced abundance in tumor-bearing mice. Thus HIF-1α acts as a metabolic switch for Tregs between glycolytic-driven migration and oxidative phosphorylation-driven immunosuppression.

Graphical Abstract

This is an open access article under the CC BY-NC-ND license (http://creativecommons.org/licenses/by-nc-nd/4.0/).

*Correspondence: maciej.lesniak@northwestern.edu.

AUTHOR CONTRIBUTIONS

J.M. and M.S.L. conceived the study. J.M., C.L.-C., A.R., M.E.M., A.C., and A.L.C. designed, performed, and analyzed experiments. A.L.-R. performed all animal breeding and genotyping for the study. P.Z. blindly performed quantification of interstitial FFA measurements. W.K.P. blindly analyzed all migration assays. Y.H. provided assistance with animal surgeries and reagent preparations. M.S.L., N.S.C., and A.U.A. provided critical feedback, contributed to manuscript preparation, and oversaw the research program. All authors reviewed the manuscript and provided feedback with writing and revisions.

SUPPLEMENTAL INFORMATION

Supplemental Information can be found online at https://doi.org/10.1016/j.celrep.2019.03.029.

DECLARATION OF INTERESTS

The authors declare no competing interests.

Author Manuscript
Author Manuscript
Author Manuscript
Author Manuscript

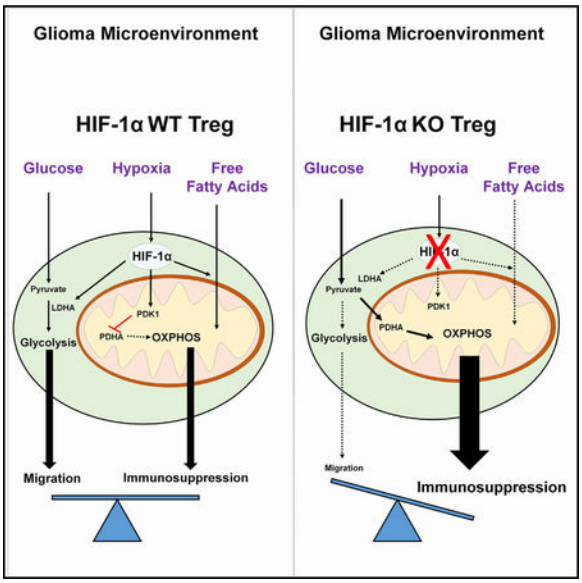

In Brief

Miska et al. demonstrate that regulatory T cell (Treg)-specific depletion of HIF-1α promotes enhanced immune suppression at the cost of migration under hypoxic conditions. Within the hypoxic brain-tumor environment, Tregs are uniquely able to metabolize extracellular free fatty acids to promote their immunosuppressive functionality, which can be targeted *in vivo*.

INTRODUCTION

Preclinical studies of glioblastoma suggest that regulatory T cells (Tregs) are pivotal for promoting tumor immunosuppression (Fecci et al., 2006; Miska et al., 2016; Wainwright et al., 2014). While previous research has established that Tregs accumulate in CNS malignancies and contribute to immunosuppression (Chang et al., 2016; El Andaloussi and Lesniak, 2007; Miska et al., 2016; Muroski et al., 2017; Wainwright et al., 2011, 2012), the mechanisms by which they thrive in the hypoxic (Dey et al., 2014) and nutrient competitive (Mirzaei et al., 2017) tumor microenvironment (TME) is not well known. Hypoxic regions are prevalent in CNS tissues and increase with the grade of malignancy (Søndergaard et al., 2002), with high-grade gliomas having more regions under chronic hypoxia than lower grade tumors (Mayer et al., 2012). Therefore, the response to hypoxia may play essential roles in T cell function in glioblastoma.

The prototypical effector of the hypoxic response, hypoxiainducible factor 1α (HIF-1α), is highly active in glioblastoma patients (Mayer et al., 2012). Furthermore, HIF-1α has been previously identified to correlate positively with the grade, invasion, and progression of glioma (Evans et al., 2004; Zagzag et al., 2000). HIF-1α has pleiotropic effects, with wide-ranging effects on angiogenesis (Krock et al., 2011), glycolysis (Robey et al., 2005), and cell survival under reduced oxygen conditions (Semenza, 2002). Other studies have demonstrated that HIF-1α regulates lipid uptake, which is a potent survival mechanism for

Author Manuscript Author Manuscript Author Manuscript Author Manuscript

tumors (Bensaad et al., 2014). These studies suggest that HIF-1α may endow Tregs with metabolic properties that allow them to endure within the tumor.

The effect of hypoxia on Treg function is conflicting. Dang et al. (2011) demonstrated that the canonical hypoxia sensor, HIF-1α, negatively regulates Foxp3 expression while promoting TH17 differentiation. Other studies have also lent credence to the Treg-inhibitory actions of HIF-1α (Hsiao et al., 2015; Hsu and Lai, 2018). However, other studies have shown that HIF-1α positively affects Treg function (Ben-Shoshan et al., 2008; Clambey et al., 2012) and plays a role in their suppressive function in tumors (Westendorf et al., 2017). This dichotomous nature reflects a complicated role of HIF-1α in immunosuppression, which may provide critical insight into how these cells function. Furthermore, it is unknown how HIF-1α mechanistically leads to enhanced or diminished Treg function within tumors.

HIF-1α inhibits mitochondrial function to prevent oxidative stress from killing cells in oxygen-restricted environments (Majmundar et al., 2010). However, the exact interplay between HIF-1α and the metabolic choice of Tregs is unknown. Interestingly, a recent study has shown that Tregs will utilize lipid metabolism to thrive in poor glucose environments (Pacella et al., 2018), suggesting that lipid metabolism may be responsible for their survival within tumors. The metabolic properties of Tregs *in vivo* are still a highly contentious topic. While no scientific consensus exists (Newton et al., 2016), a constant among studies is that catabolic (Issa, 2017), mitochondria-driven oxidative phosphorylation (Angelin et al., 2017; Beier et al., 2015) is critical for Treg functionality. The metabolic choices of Tregs in the context of glioma are unknown and may provide novel avenues to enhance immunotherapy.

Herein, utilizing an animal model with Treg-specific ablation of HIF-1α, we reveal that hypoxia promotes the migration of Tregs at the expense of their suppressive function. Under hypoxia, the suppressive function of Tregs is maintained by the lipid uptake and/or oxidation program, which is critical to Treg function both *in vitro* and *in vivo*. These findings resolve the discrepancies in the role of HIF-1α in Tregs, proving that it promotes migration over suppression.

RESULTS

Ablation of HIF-1α in Tregs Causes Enhanced Mitochondrial Metabolism

We first crossed Foxp3-YFP-CRE mice to HIF-1α Flox mice to generate a Treg-specific deletion of HIF-1α (termed hereinafter as HIF-1α [knockout] KO) to probe the role of this canonical hypoxic sensor to both glycolytic and oxidative phosphorylation (OXPHOS)-driven Treg metabolism. We first sought to understand the mitochondrial metabolic choices Tregs make under hypoxia and how the deficiency of HIF-1α regulates this process in Figure 1. HIF-1α WT (Foxp3-YFP-CRE mice used as wild-type [WT] throughout the paper) or HIF-1α KO Tregs were FACS (fluorescence-activated cell sorting) sorted, expanded, and incubated in 21% (normoxia) or 1% (hypoxia) oxygen (O_2) overnight before a mitochondrial stress test was performed utilizing an extracellular flux analyzer. Palmitate was added as an initial injection, because previous work has shown that Tregs may utilize exogenous fatty acid (FA) uptake for their stability and/or function (Berod et al., 2014; Muroski et al., 2017). Surprisingly, not only did HIF-1α KO Tregs have a higher basal oxygen consumption rate

Author Manuscript Author Manuscript Author Manuscript Author Manuscript

(OCR), maximal OCR, and ATP-linked respiration than control Tregs under normoxia, but they also maintained the same phenotype, even under extreme hypoxia (Figures 1A and 1B). Importantly, under conditions of hypoxia, HIF-1α WT Tregs upregulated OCR with palmitate injection (−0.75 ± 3 versus 6 ± 4 pmol of O_2 per minute in normoxia versus hypoxia, respectively), while HIF-1α KO Tregs had no change in palmitate-induced OCR, despite having a generally higher amount of palmitate-induced OCR.

Bulk metabolomics data confirmed enhanced citrate, malate, and fumarate with a concomitant decrease in lactate within HIF-1α KO Tregs, compared to HIF-1α WT Tregs, under hypoxia (Figure S1A) but not normoxia (Figure S1B). However, freshly sorted Tregs from spleens of both HIF-1α WT and HIF-1α KO tumor-bearing mice did not show any significant changes in metabolite content, suggesting that the TME drives metabolic change in Tregs (Figure S2). In summation, these data indicate that HIF-1α restricts the mitochondrial metabolism of glucose by Tregs under hypoxia. As we saw a significant increase in palmitate-induced OCR by Tregs under hypoxia, the data suggest that, under hypoxia (like conditions within the TME), Tregs may utilize lipids to perform their metabolic functions. As the mitochondrion is considered to be the central regulator of the immunosuppressive capabilities of Tregs (Gerriets et al., 2015), we next sought to understand how specific ablation of HIF-1α influenced Treg function.

Deletion of HIF-1α Enhances Treg-Mediated Immunosuppression under Hypoxia

To understand how ablation of HIF-1α influences canonical Treg function, we sorted and expanded Tregs and performed a series of T cell suppressor assays with the same pool of $CD8^+$ T cells as responders in Figure 2. There was no change in the suppressive function of Tregs under 21% O_2 (Figure 2A). Surprisingly, under conditions of hypoxia, HIF-1α KO Tregs were significantly enhanced in their ability to suppress T cell proliferation (Figure 2B). At Treg:CD8 ratios of 1:1, 1:2, and 1:4, the total proliferation of $CD8^+$ T cells was dramatically inhibited ($p < 0.001$) by HIF-1α KO Tregs, which was also reflected by the reduced $CD8^+$ T cell expansion index (Figure 2B, right). As hypoxic signaling is known to upregulate glycolysis by shuttling pyruvate away from the mitochondria to produce more lactate (Semenza, 2010), it is possible that HIF1α KO Tregs are shuttling more glucose into the mitochondria to enhance their suppressive function in hypoxia. Therefore, we attempted to rescue improved Treg suppression by an inhibitor of pyruvate import into the mitochondria, UK5099 (Bricker et al., 2012). Pre-treatment of HIF-1α KO Tregs with UK5099 (10 μM) abrogated the enhanced suppression of HIF-1α KO Tregs under hypoxia, as measured by $CD8^+$ T cell expansion index (Figure 2C). We also treated HIF-1α WT Tregs with dichloroacetate (DCA), a PDK1 inhibitor that promotes mitochondrial function over glycolysis (Xie et al., 2011), to mimic the effects of HIF-1α KO (Figure 2D). Tregs pretreated with DCA were significantly better at suppressing T cell proliferation than HIF-1α WT Tregs. These results suggest that HIF-1α restricts glucose oxidation, which stymies Treg immunosuppression. We next sought to dissect the role that lipid OXPHOS has on Treg function and its relevance to Treg metabolism in brain tumors. Furthermore, we sought to understand whether HIF-1α plays a role in these metabolic decisions.

Author Manuscript Author Manuscript Author Manuscript Author Manuscript

Inhibition of Lipid Uptake and/or Oxidation Prevents Treg Immunosuppressive Capabilities

In vitro inhibition of fatty acid oxidation (FAO) with Etomoxir (Eto) (also recently shown to induce oxidative stress in T cells; O'Connor et al., 2018), enhanced the relative Treg abundance of CD3-stimulated splenocytes and also enhanced Treg abundance under Treg-inducing conditions (+transforming growth factor β1 [+TGF-β1]) (Figure S3A), which is in contrast to previous studies (Michalek et al., 2011). However, treatment with the irreversible inhibitor of fatty acid transport, sulfo-N-succinimidyl oleate (SSO) (Kuda et al., 2013), resulted in a significant inhibition in the relative abundance of Tregs. However, there was a consistent change in the expression of many suppressive markers by sorted and expanded Tregs (Figure 3A). In particular, both Eto and SSO treatment significantly inhibit Granzyme B, CD39, and NRP1 expression by Tregs ($p < 0.001$). These results suggest that free fatty acids (FFAs) may be needed for the generation of immune suppression within tumors.

As inhibition of lipid uptake and/or oxidation perturbs proteins important to Treg functionality, we determined whether this influenced Treg suppressive abilities (Figures 3B–3G). Expanded Tregs maintained at least 95% of their $Foxp3^+$ expression after 48 h of treatment with both inhibitors (which is comparable to controls), suggesting that inhibition of lipid oxidation (Eto) (Figure 3B) or palmitate uptake (SSO) (Figure 3E) does not affect the stability of Foxp3. Pre-treatment with either drug did not affect Treg viability (Figure S3B). Inhibitor pre-treated Tregs were extensively washed and co-cultured at different ratios with proliferation-dye-labeled $CD8^+$ T cells for 72 h (Figures 3C, 3D, 3F, and 3G). Both treatments resulted in an approximately 2-fold reduction of Treg-mediated suppression at most ratios tested. The results show that Treg-mediated immunosuppression is enforced by lipid uptake and oxidation. We performed these assays under hypoxia, with both HIF1α WT and HIF-1α KO Tregs to understand the importance of HIF-1α signaling on lipid dependence by Tregs (Figures 3H and 3I). Importantly, the ability of HIF-1α KO Tregs to suppress T cell expansion was unaffected by pre-treatment with either Eto or SSO. This suggests that HIF-1α promotes reliance on FFA by Tregs for the promotion of immunosuppression.

Inhibition of Lipid Metabolism Influences the Mitochondrial Function of Tregs *In Vitro*

We next sought to understand how perturbations in lipid metabolism affect the mitochondrial function of Tregs and how HIF-1α may be regulating this. Pre-treatment of Tregs with Eto decreased maximal respiration of both HIF-1α WT and HIF-1α KO Tregs under normoxia, with no significant changes in basal OCR or ATP-linked respiration (Figures S4A and S4B). However, under hypoxia, HIF-1α WT Tregs were significantly more affected by Eto treatment than HIF-1α KO Tregs: the basal OCR of only HIF-1α WT Tregs was changed only under hypoxia (84 ± 10 versus 66 ± 10 pmol of O_2 per minute in control versus Eto-treated Tregs, respectively), and their maximal OCR was more significantly affected than that of HIF-1α KO Tregs (Figures 4A and 4B) (70% ± 10% reduction in HIF-1α WT and 30% ± 3% in HIF-1α KO Tregs, $p < 0.0027$). Of note, Eto pre-treatment increased palmitate-induced OCR in both groups, suggesting that inhibition of lipid oxidation promotes its own subsequent import.

Author Manuscript Author Manuscript Author Manuscript Author Manuscript

As an alternative approach, we performed the same assays using SSO (Figure S4). SSO treatment had minimal effects on mitochondrial metabolism, with the interesting exception that treatment with SSO abolished the increase in palmitate-induced OCR in HIF-1α KO Tregs under both normoxia and hypoxia ($p < 0.001$) but not in HIF-1α WT Tregs. As HIF-1α is known to shuttle exogenous FFA into lipid droplets (and away from the mitochondria), enhanced mitochondrial consumption of palmitate by HIF-1α KO Tregs under hypoxia fits with our current knowledge (Bensaad et al., 2014). The results of these experiments suggest that Tregs may utilize lipid metabolism for mitochondrial function under hypoxia, so we next sought to understand the contribution of lipid metabolism to Treg-mediated immunosuppression.

Tregs Prefer Fatty Acid Uptake within Brain Tumors

To determine the metabolic preferences of T cell subsets within the glioma microenvironment, we implanted Foxp3-YFP mice intracranially with the murine GL-261 glioblastoma tumor model and, after 2 weeks of tumor engraftment, performed flow-cytometric analysis on infiltrating T cells (Figures 4C and 4D). Differences in the percentage of cells taking up the quantum-dot 605 (Qdot605)-conjugated palmitic acid biosensor (Muroski et al., 2017) and the mean fluorescence intensity (MFI) of uptake (Figure 4C) reveal that Tregs uptake dramatically more fatty acid in comparison to both $CD8^+$ and $CD4^+$ conventional T cells (***$p < 0.001$). These observations are consistent with our previous results (Muroski et al., 2017). As glucose uptake can provide alternative fuel for mitochondrial metabolism, we also examined the T cell uptake of glucose using a fluorescent glucose analog (2-NBDG) (Zou et al., 2005). 2-NBDG uptake showed a relatively low amount of glucose uptake by all T cell subsets (2%–8%); effector $CD4^+$ T cells had the highest percentage of cells taking up glucose (*$p < 0.05$), while Tregs had the highest MFI of 2-NBDG (*$p < 0.05$) (Figure 4D).

While glucose uptake is variable across T cell subsets, the dramatic increase in lipid uptake by Tregs highlights the potential utilization of FFA by Tregs within the TME. Interestingly, analysis of interstitial non-esterified FFA was 3.2-fold higher within the tumor-bearing hemisphere, as compared to the hemisphere without tumor (Figure 4E). The results of these experiments suggest that Tregs may be preferentially utilizing fatty acid uptake and/or oxidation for metabolism in the TME and that the prerequisite substrates are abundant.

FFA uptake from the extracellular environment is known to be mediated by specific fatty acid transporters (Glatz et al., 2010). We sought to determine the expression of fatty acid transporters on T cell subsets within the tumor tissue, as previous work has shown that Tregs prefer exogenous FA for their metabolic needs (Berod et al., 2014). Examination of all three established surface fatty acid transporters, CD36, SLC27A1, and SLC27A4 (Glatz et al., 2010), revealed a higher percentage of Treg cells expressing fatty acid transporters on the cell surface compared to other T cell subsets. As shown in Figure 4F, Tregs are enriched in the surface expression of CD36, as compared to $CD4^+Foxp3^-$ and $CD8^+$ T cell populations, but was not significant in the periphery. Figure 4F shows that the SLC27A1 also was enriched in tumoral Tregs. There is no change in the expression of SLC27A4, suggesting specific surface fatty acid transporter upregulation in the tumor. While all T cells had an

Author Manuscript Author Manuscript Author Manuscript Author Manuscript

upregulation of fatty acid transporters in the brain, Tregs had proportionally more expression, suggesting that they are more sensitive to FA metabolic alteration.

Inhibition of Lipid Oxidation Prevents Immunosuppression in a Murine Model of Glioblastoma

Eto has been previously shown to enhance animal survival in an immunocompetent animal model of glioma (Lin et al., 2016). Our data showed no influence on the viability or metabolic uptake of any glioma line tested (Figure S5). Thus, we determined whether Eto treatment inhibited immunosuppression of mice harboring brain tumors. As demonstrated in Figure 5A, C57BL/6 mice had a significant increase in survival (**$p < 0.01$), with a median survival of 20 and 25 days in control versus intracranial Eto treatment, respectively. In Rag-1 KO mice, which are deficient in T and B cells, there was no significant change in survival, and both groups had a median survival of 22 days (Figure 5A, right). In Figure 5B, Eto-treated groups had a favorable increase in both CD4:Treg and CD8:Treg ratios, as compared to control tumor subsets, which is predictive of therapeutic efficacy (Curran et al., 2010). Eto treatment caused a significant decrease in tumor Tregs compared to the control group (**$p < 0.01$). These results suggest that Eto treatment has an impact on the microenvironment by inhibition of immunosuppression.

If the significant target of fatty acid oxidation inhibition is on the adaptive immune compartment, then targeting fatty acid oxidation in the periphery may yield results similar to those for intracranial treatment. To test the possibility that peripheral inhibition of fatty acid oxidation enhances animal survival, we injected Eto peripherally every day into tumor-bearing mice, starting 5 days after tumor implantation. As demonstrated in Figure 5C, HIF-1α WT mice had a significant increase in survival (**$p < 0.01$) in groups treated intraperitoneally (i.p.) with Eto versus control groups. Figure 5D shows that the Eto-treated groups had a favorable increase in both CD4:Treg and CD8:Treg ratios, **$p < 0.01$ and *$p < 0.05$, respectively. The total Treg number is decreased in the Eto-treated group compared to the control group ($p < 0.09$) as well as the percentage of $CD4^+Foxp3^+$ T cells. These results suggest that Eto treatment has an impact on systemic immunity against glioma. Lastly, peripheral Eto treatment in HIF1α KO mice bearing tumors had no change in Treg recruitment (Figure S6A).

HIF-1α Promotes Glycolysis, Enhancing Treg Migratory Capabilities

As we saw that HIF-1α KO is potentially shuttling more pyruvate into the mitochondria under hypoxia (Figure 2C)—and, thus, away from lactic acid production—we measured extracellular acidification induced by hypoxia (Figure 6). HIF-1α WT Tregs had a significantly increased extracellular acidification rate (ECAR) under hypoxia (49 ± 2 mpH/min versus 66 ± 4 mpH/min in normoxia versus hypoxia, respectively). Interestingly, not only did HIF-1α KO Tregs have a lower ECAR compared to controls under normoxia (49 ± 2 mpH/min versus 26 ± 1 mpH/min in HIF-1α WT versus HIF-1α KO Tregs, respectively), but also the ECAR was unaffected by hypoxia (26 ± 1 mpH/min versus 26 ± 2 mpH/min in normoxia versus hypoxia, respectively) (Figures 6A and 6B). Treatment of Tregs with oligomycin reveals the maximal glycolytic capacity of these cells, which highlights a permanent decrease in the glycolytic metabolism in HIF-1α KO Tregs ($p <$

Author Manuscript Author Manuscript Author Manuscript Author Manuscript

0.001) (Figure 6B, right). qPCR of two central regulators of glycolytic metabolism PDK1 and LDHA were upregulated by 4- and 2-fold, respectively, under hypoxia treatment. This effect was abolished in HIF-1α KO Tregs (Figure 6C). Critically, pretreatment of Tregs with the PDK1 inhibitor DCA induced significant decreases in both basal and maximal ECAR (Figure 6D), with a concomitant increase in basal and maximal OCR (Figure 6E), mimicking the effects of HIF-1α deficiency on Treg metabolism.

A recent study highlighted the need for glycolysis in the migratory capabilities of Tregs (Kishore et al., 2017). To address the migratory capabilities of Tregs, we sorted and expanded HIF-1α KO Tregs and HIF-1α WT Tregs *in vitro* before performing overnight Transwell migration assays (Figure 6F). HIF-1α KO Tregs were significantly stymied in their migration to both a glioma-produced Treg-chemotactic cytokine CCL22 (Jordan et al., 2008)(88.5 ± 2.1 HIF-1α WT versus 44 ± 1.2 HIF-1α KO; $p \leqslant 0.001$) or cultured GL-261 (83 ± 4.8 HIF-1α WT versus 47.9 ± 6.8 HIF-1α KO; $p \leqslant 0.001$). Pre-treatment of Eto had no effect on the *in vitro* migration of HIF-1α WT or HIF-1α KO Tregs (Figure S6B). Critically, extracellular flux analysis showed that pulsing with CCL22 induces significantly more glycolytic metabolism in HIF-1α WT Tregs as compared to HIF-1α KO Tregs (Figure 6G).

HIF-1α Controls Tumor-Infiltrating Tregs' Migratory Capacity *In Vivo*

To determine whether this migratory perturbation is occurring *in vivo*, we sorted and expanded HIF-1α WT or HIF-1α KO Tregs, labeled with two different stable fluorescence tags and mixed at a 1:1 ratio before being injected intravenously (i.v.) into tumor-bearing mice (Figure 7A). After 48 h, organs were harvested, and the ratio of HIF-1α WT:KO Tregs was assessed (Figure 7B). While the ratios of Tregs in the spleen and draining lymph node (DLN) were 1:1 and 1:1.4, respectively, in the tumor, HIF-1α WT Tregs were 3.2-fold higher ($p < 0.001$) than HIF-1α KO Tregs. We also pre-treated Tregs with DCA and performed the same competition assay, which also revealed reduced Treg infiltration into the tumor (Figure S7C). These data demonstrate a reduced infiltrative capability of Tregs deficient in HIF-1α.

Implantation of the murine syngeneic GL-261 astrocytoma model into HIF-1α WT and HIF-1α KO mice revealed a small but significant increase in animal survival in HIF-1α KO animals ($p \leqslant 0.01$), as shown in (Figure 7C). Immune infiltrate analysis at 14 days after tumor implantation shows a specific decrease in the number of $Foxp3^+CD4^+$ T cells (Figure 7D) in the tumor, with no observable changes in effector $CD4^+$ or $CD8^+$ T cell numbers (Figure S7A). Interestingly, reduction in Treg numbers is only apparent in the CNS, suggesting that the influence of HIF-1α on Tregs is geographically related to the glioma. Measurement of known Treg chemokine receptors was unchanged on HIF-1α WT Tregs compared to HIF-1α KO Tregs (Figure S7B). Lastly, immunofluorescence of $Foxp3^+$ T cell infiltrates after 2 weeks of tumor growth revealed a significant reduction in Treg numbers within the tumors of mice (Figure 7E).

Author Manuscript Author Manuscript Author Manuscript Author Manuscript

DISCUSSION

The microenvironment of glioma is harsh for the survival of cells, yet Tregs persist despite these challenges. The results of this study not only broaden our knowledge of Treg biology in the context of glioma but also reveal the competition between the migratory and functional needs of these specialized cells.

Perhaps the most well-known study on the function of HIF-1α and Tregs is by Clambey et al. (2012). In this study, they show that HIF-1α is important for the function and survival of Tregs in inflamed tissues. Specifically, HIF-1α can bind to the $Foxp3^+$ promoter, is induced by hypoxia, and can prevent colitis in an adoptive transfer model of HIF-1α deficiency (Clambey et al., 2012). However, other studies suggest that HIF-1α is deleterious to Treg function. For example, other studies have shown that HIF-1α binds to Foxp3, degrading it (Dang et al., 2011), or that HIF-1α broadly downregulates Treg function (Hsiao et al., 2015). We believe that our study reconciles many of these observations.

First, we determined that HIF-1α KO Tregs suppress better than HIF-1α WT Tregs under hypoxia, a notion in line with studies that suggest that HIF-1α antagonizes $Foxp3^+$ suppressive function (Hsiao et al., 2015; Hsu and Lai, 2018). Our results confirm that the immune suppressive capabilities of Tregs require mitochondrial metabolism, which has also been previously suggested (Gerriets et al., 2015). Our data support this by showing that deficiency of HIF-1α prevents pyruvate from being shuttled to lactate production, resulting in overactive mitochondrial metabolism. The model also helps us understand previous studies suggesting that fatty acid metabolism is critical for Treg function. Many previous studies have suggested that exogenous lipids (Berod et al., 2014) and subsequent lipid oxidation are metabolically relevant for Tregs (Gerriets et al., 2015; Howie et al., 2017; Michalek et al., 2011); however, HIF-1α KO Treg resistance to Eto treatment highlights that Treg dependence on lipids is context dependent. Indeed, under the context of hypoxia, Treg suppression is severely affected by the inhibition of lipid metabolism. Therefore, under hypoxic situations, HIF-1α does, indeed, inhibit Treg suppression, but the presence of FFA in the TME promotes their suppressive functionality.

Several decades-old studies initially highlighted the presence of FFAs in the glioblastoma microenvironment (Gopal et al., 1963; Martin et al., 1996; Stein et al., 1963). Not only do our data agree with this, but it also appears that Tregs utilize this fuel in an environment in which few other substrates are available. Through several lines of evidence, we show that Tregs uptake more lipids and have the transportation machinery required for this uptake, which is in agreement with a very recent study showing that Tregs can utilize fatty acid metabolism as a complement to glycolysis (Pacella et al., 2018). This then suggests that inhibition of fatty acid metabolism in the glioma microenvironment could stymie Treg function.

As Eto has been recently shown to have various effects independent of preventing lipid transport into mitochondria, verification using another inhibitor was critical to our study. By showing that inhibition of palmitate uptake, utilizing SSO, also inhibits Treg function, we are validating a core ideology of Treg suppressive function, the necessity of lipid

Author Manuscript Author Manuscript Author Manuscript Author Manuscript

metabolism. It also shows that Treg will, indeed, utilize exogenous fatty acids for their mitochondrial function and substantiates the framework of this study. The resistance of HIF-1α-deficient Tregs to both of these inhibitors provides essential evidence that hypoxic signaling is central to this metabolic decision.

Our study also elucidates the role that FA metabolism has on immunosuppression within the brain TME. This study provides evidence that a temporary change in lipid metabolism is enough to augment the immunosuppression of glioma. Other research has suggested that this mechanism is through the effects on cancer cells in the microenvironment, which, no doubt, can play a critical role in tumor progression (Berge et al., 2003; Lin et al., 2016). However, through the use of Rag-1 KO mice, which lack T cells and B cells, the survival effect is negated, suggesting that the immune function is critical to the survival effects of fatty acid oxidation inhibition.

Lastly, we show in our murine model of glioma that ablation of HIF-1α leads to enhanced animal survival due to the decrease in the migratory abilities of HIF-1α KO Tregs. A recent study suggests that glucokinase (GCK)-mediated glycolysis drives Treg migration, generating quick ATP for migratory processes (Kishore et al., 2017). As HIF-1α activation promotes glycolytic processes over the import of pyruvate into the mitochondria for OXPHOS, our data show that HIF-1α is responsible for energizing the migration of Tregs.

This study demonstrates that hypoxia and HIF-1α interact to limit the suppressive function of Tregs; however, future work is critical to understand how other regulators of HIF-1α, such as mTORC1, contribute to Treg function or migration in brain tumors or how this pathway is controlled in Tregs compared to conventional T cell subsets. In summation, this study provides a clear picture in which HIF-1α can promote the migration of Tregs at the expense of immune suppression and that immune suppression under hypoxia prefers lipids for fuel. Future studies will need to determine whether we can promote the lipid oxidation phenotype of effector immune cells to thrive within CNS tumors, as was previously shown in a model of melanoma (Zhang et al., 2017). We hope that the interrogation of any of these strategies may promote future therapies for this incurable disease.

STAR★METHODS

CONTACT FOR REAGENT AND RESOURCE SHARING

Further information and requests for resources and reagents should be directed to and will be fulfilled by the Lead Contact, Maciej Lesniak (maciej.lesniak@northwestern.edu).

EXPERIMENTAL MODEL AND SUBJECT DETAILS

Mice—C57BL/6 (WT), C57BL/6-Foxp3-YFP-CRE, RAG1$^{0/0}$, C57BL/6-HIF-1α$^{flox/flox}$ were obtained and bred from Jackson Laboratories and housed in Northwestern University animal facility at the Center for Comparative Medicine (CCM). Foxp3-YFP-CRE was crossed with C57BL/6 HIF-1α-flox to generate Treg specific knockout of HIF-1α. Crossing was verified with genotyping using primers designed and validated by Jackson Laboratories. Mice aged 6–10 weeks were used for all experiments. Animal survival was conducted following endpoint protocols outlined in our approved animal protocols by CCM. All

Author Manuscript Author Manuscript Author Manuscript Author Manuscript

experimental protocols followed NIH guidelines and were approved by the institutional animal care and use committees (IACUC) at Northwestern University. For any and all experiments using HIF-1α-Treg KO mice, we used age and gender matched Foxp3-YFP-CRE mice as WT controls throughout the manuscript. Both male and female mice were used for all experiments. In any primary cell cultures or assays, controls were age matched and sex matched for every experiment.

Cells—The GL-261 glioma cell lines were directly purchased from NCI and cultured in DMEM (Fisher, Hampton, NJ), 10% FBS (Hyclone) with penicillin/streptomycin (Invitrogen). GL-261 is a malignant glioma cell line that is syngeneic to C57BL/6 mice (the sex of the originating tumor is Male) and was administered via intracranial injection using a stereotactic apparatus at a concentration of 2×10^5 GL-261 cells in 2.5 μL PBS (Sigma, St Louis, MI) at 6–10 weeks of age as described previously (Miska et al., 2016). Cell Lines GBM6 (Age/Sex:65/Male) and GBM12 (Age/Sex:85/Male) were obtained from C. David James Laboratory, and MES83 (Age/Sex:unknown/Female) were obtained from Ichiro Nakano, University of Alabama at Birmingham through Shi-Yuan Cheng at Northwestern University. Human cell lines were cultured in 1% FBS/DMEM. For *in-vitro* assays of proliferation, dye uptake, and cell death all cells were plated at a density of 5×10^4 per well in a 96 well plate for all assays.

METHOD DETAILS

Treg culture isolation—Splenocytes were harvested into single cell suspension from C57BL/6-Foxp3-YFP-CRE or C57BL/6-Foxp3-YFP-CRE-HIF-1α KO age and gender matched mice. Pre-enrichment of T cells was performed using the Magni-sort T cell enrichment kit (Fisher) including anti-CD8 biotin for depletion (Biolegend). Enriched cells were then sorted using a BD FACS Aria II cell sorter (Becton Dickinson, Franklin Lakes, NJ) using CD4-APC and $Foxp3^+YFP^+$ expression, then expanded with Dynabeads (Invitrogen) T cell expander beads and 2000U/ml recombinant IL-2 (Peprotech). For hypoxia treatment, Tregs from control or HIF-1α-Treg KO mice were plated overnight in 1% O_2 or 21% O_2 for gene expression or flux analysis. In experiment with flux analyses, drugs were added immediately before assay initiation. Sorted and expanded Tregs were used for suppressor assays, extracellular flux analyses, and migration assays are as described below.

In-vitro T cell suppressor/proliferation assays—For suppressor assays, Tregs were treated with inhibitors for 24 hours before being washed 3X and subsequently co-cultured (at decreasing ratios) with freshly-isolated, CTV-labeled $CD8^+$ T cells, Dynabeads (1:3 bead/T cell ratio), and 30U/ml of recombinant IL-2 (Peprotech) for 72 hours. After 72 hours (96 hours for 1% O_2 suppressors), T cells were harvested, labeled with APC-efluor780 viability dye (Ebioscience), followed by staining with appropriate flow cytometry antibodies immediately before flow cytometric analysis.

Flow cytometry analysis—For *in-vitro* studies the following flow cytometry panel was used in conjunction with CTV and viability dye: anti-CD3 Alexa700, CD4 PE-Cy7, CD8 APC, CD44 PE all at a 1:200 dilution purchased from Biolegend. For *in-vivo* and *ex-vivo*

Author Manuscript Author Manuscript Author Manuscript Author Manuscript

studies, the following flow cytometry panel was used: anti-CD3 PE-Cy7, CD4 Pacific Blue, CD8 APC, CD44 PE, and anti-CD25 Alexa 700 all at a 1:200 dilution (except anti-CD25 at a 1:50 dilution) and were purchased from Biolegend. Endogenous Foxp3 expression was detected via eYFP fluorescence (or re-stained with anti-Foxp3 Efluor-450 clone FJK-16 s for any overnight staining (Fisher)), all acquisition was performed using a BD Fortessa flow cytometer. For surface FA transporter measurement, anti-CD36-APC (Biolegend), SLC27A1 (sigma), and SLC27A4 was purchased from Abcam (Cambridge, UK), followed by secondary goat anti-rabbit IgG Alexa-647 (Jackson Immunoresearch, West Grove, PA). Proliferation was analyzed using both FACS DIVA software as well as FlowJo software to determine expansion indexes.

Immunofluorescence—After 14 days tumor engraftment, tumors from WT and KO mice were flash frozen in OCT (Fisher) and sectioned into 8μm slices using a CM1860 cryostat (Leica, Wetzlar, Germany). Sections were fixed in pre-chilled acetone then stained overnight at 4°C with 1:100 Foxp3-Biotin (Ebioscience) and Laminin-Alexa Fluor 647 1:500 (Novus, Littleton, CO) in antibody staining buffer - 0.5% Triton X-100 and 1% BSA (Sigma) in TBS (Boston Bioproducts, Ashland, MA). The following day, Streptavidin Alexa Fluor-488 (Fisher) was added for 2 hours at RT, washed, and mounted using Fluoroshield with DAPI (Sigma). Images were taken with a Leica DMi8 microscope with a 20X objective. Data was processed and quantified using imageJ.

Extracellular flux analysis—Metabolic rate of Tregs was determined via the Agilent Seahorse mitochondrial stress test assay modified with an initial palmitate injection (Santa Clara, CA). Briefly, expanded Tregs were cultured for 4 hours in substrate-limited medium (Kreb's/HEPES Buffer) before being adhered to a Agilent Seahorse XF96 cell culture microplate with Cell Tak (Corning, Corning, NY) at a density of2.5×10^5 Tregs/well which were then washed with fatty acid media (the day of the assay in a 96-well assay plate)(Wang et al., 2013). The stress test for Tregs was performed by injection of Palmitate-BSA before the injections of all standardized reagents for the mitochondrial stress test as described in the protocol. CCL22 (Peprotech) was injected at a final concentration of 100 ng/ml to measure ECAR over time. All reagents for the mitochondrial stress test, including Palmitate-BSA and BSA controls, were purchased from Agilent.

Migration assays—To determine the *in-vitro* migration of Tregs, expanded Tregs were cultured overnight in 5% reduced serum RPMI before being plated at a density of 2.5×10^5 Tregs/well in the top chamber of 3μm transwell inserts (Corning). The bottom wells were either seeded with 5×10^4 GL-261 overnight or plated with 5% FBS RPMI supplemented with 100ng/ml recombinant murine CCL22 (Peprotech). Tregs were allowed to migrate overnight at 1% O_2 before migration was assessed. Both cells in the top chamber and bottom chamber were manually counted by a blinded researcher (W.K.P.) to validate migration. For *in-vivo* migration of Tregs, expanded Tregs were labeled with eBioscience Cell Proliferation Dye eFluor 450 (HIF-1α WT Tregs) or eFluor 670 (HIF-1α KO Tregs), mixed at a 1:1 ratio, and injected *i.v.* (2.5×10^6 of each Treg) into GL-261 tumor-bearing mice one week after injection. After 48 hours, cells were isolated from brains, spleen, and DLNs of mice, stained

Author Manuscript Author Manuscript Author Manuscript Author Manuscript

with markers for CD4-Percp-Cy5.5 and CD45-PE, and ratios of labeled Tregs were analyzed.

QUANTIFICATION AND STATISTICAL ANALYSIS

Statistical significance across two group was determined using two-tailed unpaired Student's t test performed on Figures 1A, 2A–2B (left), 2D, 3D, 3G, 4D, 5B, 5D, 6D–6G, 7D–7E, S1, S2, S5, and S7A–S7B. One-way ANOVA with Tukey's post hoc was performed on Figures 1B, 2A and 2B (right), 2C, 3H, 3I, 4B–4D, 4F, 6B–6C, 7B (right), S3A–S3B, S4B, S4D, S4F, S6A–S6B, and S7C for comparisons of 3 or more groups. Kaplan Meier curves were generated and the Log rank test was performed for analysis of *in-vivo* survival rate (Figure 5A, 5C, and 7C). p values were calculated in Prism software (Graphpad, San Diego, CA) and the significance are as stated in the figure legends. Error bars shown as ± the Standard Error of the Mean (SEM) for all figures. Immunofluorescence images were processed in ImageJ

DATA AND SOFTWARE AVAILABILITY

Raw and analyzed data has been submitted to the Mendeley database and is available using following doi: https://doi.org/10.17632/k8z9vbmddc.1 Direct weblink to Mendeley datasets: https://data.mendeley.com/datasets/k8z9vbmddc/1

Supplementary Material

Refer to Web version on PubMed Central for supplementary material.

ACKNOWLEDGMENTS

We would like to thank Peng Gao at the Metabolomics Core Facility at Northwestern University (NU) for performing bulk metabolomics and the NU Flow Cytometry Core for the use of their flow cytometry sorters and analyzers. We would also like to thank Ana Berce and Irina Balyasnikova for critical review of the manuscript. Financial support comes from an Outstanding Investigator Award from NIH/NCI to M.S.L. (R35CA197725), a grant from NIH/NINDS to M.S.L. (R01NS093903), and an Outstanding Investigator Award from NIH/NCI to N.S.C. (R35CA197532). J.M. received a fellowship from the NIH/NCI (1F32NS098737–01A1).

REFERENCES

Angelin A, Gil-de-Gómez L, Dahiya S, Jiao J, Guo L, Levine MH, Wang Z, Quinn WJ 3rd, Kopinski PK, Wang L, et al. (2017). Foxp3 reprograms T cell metabolism to function in low-glucose, high-lactate environments. Cell Metab 25, 1282–1293.e7. [PubMed: 28416194]

Beier UH, Angelin A, Akimova T, Wang L, Liu Y, Xiao H, Koike MA, Hancock SA, Bhatti TR, Han R, et al. (2015). Essential role of mitochondrial energy metabolism in Foxp3^{+} T-regulatory cell function and allograft survival. FASEB J 29, 2315–2326. [PubMed: 25681462]

Ben-Shoshan J, Maysel-Auslender S, Mor A, Keren G, and George J (2008). Hypoxia controls CD4+CD25+ regulatory T-cell homeostasis via hypoxia-inducible factor-1alpha. Eur. J. Immunol 38, 2412–2418. [PubMed: 18792019]

Bensaad K, Favaro E, Lewis CA, Peck B, Lord S, Collins JM, Pinnick KE, Wigfield S, Buffa FM, Li JL, et al. (2014). Fatty acid uptake and lipid storage induced by HIF-1α contribute to cell growth and survival after hypoxia-reoxygenation. Cell Rep 9, 349–365. [PubMed: 25263561]

Berge K, Tronstad KJ, Bohov P, Madsen L, and Berge RK (2003). Impact of mitochondrial beta-oxidation in fatty acid-mediated inhibition of glioma cell proliferation. J. Lipid Res 44, 118–127. [PubMed: 12518030]

Author Manuscript Author Manuscript Author Manuscript Author Manuscript

Berod L, Friedrich C, Nandan A, Freitag J, Hagemann S, Harmrolfs K, Sandouk A, Hesse C, Castro CN, Bähre H, et al. (2014). De novo fatty acid synthesis controls the fate between regulatory T and T helper 17 cells. Nat. Med 20, 1327–1333. [PubMed: 25282359]

Bricker DK, Taylor EB, Schell JC, Orsak T, Boutron A, Chen YC, Cox JE, Cardon CM, Van Vranken JG, Dephoure N, et al. (2012). A mitochondrial pyruvate carrier required for pyruvate uptake in yeast, Drosophila, and humans. Science 337, 96–100. [PubMed: 22628558]

Chang AL, Miska J, Wainwright DA, Dey M, Rivetta CV, Yu D, Kanojia D, Pituch KC, Qiao J, Pytel P, et al. (2016). CCL2 produced by the glioma microenvironment is essential for the recruitment of regulatory T cells and myeloid-derived suppressor cells. Cancer Res 76, 5671–5682. [PubMed: 27530322]

Clambey ET, McNamee EN, Westrich JA, Glover LE, Campbell EL, Jedlicka P, de Zoeten EF, Cambier JC, Stenmark KR, Colgan SP, and Eltzschig HK (2012). Hypoxia-inducible factor-1 alpha-dependent induction of FoxP3 drives regulatory T-cell abundance and function during inflammatory hypoxia of the mucosa. Proc. Natl. Acad. Sci. USA 109, E2784–E2793. [PubMed: 22988108]

Curran MA, Montalvo W, Yagita H, and Allison JP (2010). PD-1 and CTLA-4 combination blockade expands infiltrating T cells and reduces regulatory T and myeloid cells within B16 melanoma tumors. Proc. Natl. Acad. Sci. USA 107, 4275–4280. [PubMed: 20160101]

Dang EV, Barbi J, Yang HY, Jinasena D, Yu H, Zheng Y, Bordman Z, Fu J, Kim Y, Yen HR, et al. (2011). Control of T(H)17/T(reg) balance by hypoxia-inducible factor 1. Cell 146, 772–784. [PubMed: 21871655]

Dey M, Chang AL, Wainwright DA, Ahmed AU, Han Y, Balyasnikova IV, and Lesniak MS (2014). Heme oxygenase-1 protects regulatory T cells from hypoxia-induced cellular stress in an experimental mouse brain tumor model. J. Neuroimmunol 266, 33–42. [PubMed: 24268287]

El Andaloussi A, and Lesniak MS (2007). CD4+ CD25+ FoxP3+ T-cell infiltration and heme oxygenase-1 expression correlate with tumor grade in human gliomas. J. Neurooncol 83, 145–152. [PubMed: 17216339]

Evans SM, Judy KD, Dunphy I, Jenkins WT, Hwang WT, Nelson PT, Lustig RA, Jenkins K, Magarelli DP, Hahn SM, et al. (2004). Hypoxia is important in the biology and aggression of human glial brain tumors. Clin. Cancer Res 10, 8177–8184. [PubMed: 15623592]

Fecci PE, Sweeney AE, Grossi PM, Nair SK, Learn CA, Mitchell DA, Cui X, Cummings TJ, Bigner DD, Gilboa E, and Sampson JH (2006). Systemic anti-CD25 monoclonal antibody administration safely enhances immunity in murine glioma without eliminating regulatory T cells. Clin. Cancer Res 12, 4294–4305. [PubMed: 16857805]

Gerriets VA, Kishton RJ, Nichols AG, Macintyre AN, Inoue M, Ilkayeva O, Winter PS, Liu X, Priyadharshini B, Slawinska ME, et al. (2015). Metabolic programming and PDHK1 control CD4+ T cell subsets and inflammation. J. Clin. Invest 125, 194–207. [PubMed: 25437876]

Glatz JFC, Luiken JJFP, and Bonen A (2010). Membrane fatty acid transporters as regulators of lipid metabolism: implications for metabolic disease. Physiol. Rev 90, 367–417. [PubMed: 20086080]

Gopal K, Grossi E, Paoletti P, and Usardi M (1963). Lipid composition of human intracranial tumors: a biochemical study. Acta Neurochir. (Wien) 11, 333–347. [PubMed: 14064798]

Howie D, Cobbold SP, Adams E, Ten Bokum A, Necula AS, Zhang W, Huang H, Roberts DJ, Thomas B, Hester SS, et al. (2017). Foxp3 drives oxidative phosphorylation and protection from lipotoxicity. JCI Insight 2, e89160. [PubMed: 28194435]

Hsiao HW, Hsu TS, Liu WH, Hsieh WC, Chou TF, Wu YJ, Jiang ST, and Lai MZ (2015). Deltex1 antagonizes HIF-1α and sustains the stability of regulatory T cells in vivo. Nat. Commun 6, 6353. [PubMed: 25695215]

Hsu TS, and Lai MZ (2018). Hypoxia-inducible factor 1α plays a predominantly negative role in regulatory T cell functions. J. Leukoc. Biol 104, 911–918. [PubMed: 29901858]

Issa F (2017). Research highlights: Foxp3 and Toll-like receptor signaling balance T_{reg} cell anabolic metabolism for suppression. Transplantation 101, 218.

Jordan JT, Sun W, Hussain SF, DeAngulo G, Prabhu SS, and Heimberger AB (2008). Preferential migration of regulatory T cells mediated by glioma-secreted chemokines can be blocked with chemotherapy. Cancer Immunol. Immunother 57, 123–131. [PubMed: 17522861]

Author Manuscript Author Manuscript Author Manuscript Author Manuscript

Kishore M, Cheung KCP, Fu H, Bonacina F, Wang G, Coe D, Ward EJ, Colamatteo A, Jangani M, Baragetti A, et al. (2017). Regulatory T cell migration is dependent on glucokinase-mediated glycolysis. Immunity 47, 875–889.e10. [PubMed: 29166588]

Krock BL, Skuli N, and Simon MC (2011). Hypoxia-induced angiogenesis: good and evil. Genes Cancer 2, 1117–1133. [PubMed: 22866203]

Kuda O, Pietka TA, Demianova Z, Kudova E, Cvacka J, Kopecky J, and Abumrad NA (2013). Sulfo-N-succinimidyl oleate (SSO) inhibits fatty acid uptake and signaling for intracellular calcium via binding CD36 lysine 164: SSO also inhibits oxidized low density lipoprotein uptake by macrophages. J. Biol. Chem 288, 15547–15555. [PubMed: 23603908]

Lin H, Patel S, Affleck VS, Wilson I, Turnbull DM, Joshi AR, Maxwell R, and Stoll EA (2016). Fatty acid oxidation is required for the respiration and proliferation of malignant glioma cells. Neuro Oncol 19, 23–54.

Majmundar AJ, Wong WJ, and Simon MC (2010). Hypoxia-inducible factors and the response to hypoxic stress. Mol. Cell 40, 294–309. [PubMed: 20965423]

Martin DD, Robbins MEC, Spector AA, Wen BC, and Hussey DH (1996). The fatty acid composition of human gliomas differs from that found in nonmalignant brain tissue. Lipids 31, 1283–1288. [PubMed: 8972462]

Mayer A, Schneider F, Vaupel P, Sommer C, and Schmidberger H (2012). Differential expression of HIF-1 in glioblastoma multiforme and anaplastic astrocytoma. Int. J. Oncol 41, 1260–1270. [PubMed: 22825389]

Michalek RD, Gerriets VA, Jacobs SR, Macintyre AN, MacIver NJ, Mason EF, Sullivan SA, Nichols AG, and Rathmell JC (2011). Cutting edge: distinct glycolytic and lipid oxidative metabolic programs are essential for effector and regulatory CD4+ T cell subsets. J. Immunol 186, 3299–3303. [PubMed: 21317389]

Mirzaei R, Sarkar S, and Yong VW (2017). T cell exhaustion in glioblastoma: intricacies of immune checkpoints. Trends Immunol 38, 104–115. [PubMed: 27964820]

Miska J, Rashidi A, Chang AL, Muroski ME, Han Y, Zhang L, and Lesniak MS (2016). Anti-GITR therapy promotes immunity against malignant glioma in a murine model. Cancer Immunol. Immunother 65, 1555–1567. [PubMed: 27734112]

Muroski ME, Miska J, Chang AL, Zhang P, Rashidi A, Moore H, Lopez-Rosas A, Han Y, and Lesniak MS (2017). Fatty acid uptake in T cell subsets using a quantum dot fatty acid conjugate. Sci. Rep 7, 5790. [PubMed: 28724939]

Newton R, Priyadharshini B, and Turka LA (2016). Immunometabolism of regulatory T cells. Nat. Immunol 17, 618–625. [PubMed: 27196520]

O'Connor RS, Guo LL, Ghassemi S, Snyder NW, Worth AJ, Weng L, Kam Y, Philipson B, Trefely S, Nunez-Cruz S, et al. (2018). The CPT1a inhibitor, etomoxir induces severe oxidative stress at commonly used concentrations. Sci. Rep 8, 6289. [PubMed: 29674640]

Pacella I, Procaccini C, Focaccetti C, Miacci S, Timperi E, Faicchia D, Severa M, Rizzo F, Coccia EM, Bonacina F, et al. (2018). Fatty acid metabolism complements glycolysis in the selective regulatory T cell expansion during tumor growth. Proc. Natl. Acad. Sci. USA 115, E6546–E6555. [PubMed: 29941600]

Robey IF, Lien AD, Welsh SJ, Baggett BK, and Gillies RJ (2005). Hypoxia-inducible factor-1alpha and the glycolytic phenotype in tumors. Neoplasia 7, 324–330. [PubMed: 15967109]

Semenza GL (2002). HIF-1 and tumor progression: pathophysiology and therapeutics. Trends Mol. Med 8 (4, Suppl), S62–S67. [PubMed: 11927290]

Semenza GL (2010). HIF-1: upstream and downstream of cancer metabolism. Curr. Opin. Genet. Dev 20, 51–56. [PubMed: 19942427]

Søndergaard KL, Hilton DA, Penney M, Ollerenshaw M, and Demaine AG (2002). Expression of hypoxia-inducible factor 1alpha in tumours of patients with glioblastoma. Neuropathol. Appl. Neurobiol 28, 210–217. [PubMed: 12060345]

Stein AA, Opalka E, and Peck F (1963). Fatty acid analysis of brain tumors by gas phase chromatography. Arch. Neurol 8, 50–55. [PubMed: 13983668]

Author Manuscript Author Manuscript Author Manuscript Author Manuscript

Wainwright DA, Sengupta S, Han Y, and Lesniak MS (2011). Thymus-derived rather than tumor-induced regulatory T cells predominate in brain tumors. Neuro Oncol 13, 1308–1323. [PubMed: 21908444]

Wainwright DA, Balyasnikova IV, Chang AL, Ahmed AU, Moon KS, Auffinger B, Tobias AL, Han Y, and Lesniak MS (2012). IDO expression in brain tumors increases the recruitment of regulatory T cells and negatively impacts survival. Clin. Cancer Res 18, 6110–6121. [PubMed: 22932670]

Wainwright DA, Chang AL, Dey M, Balyasnikova IV, Kim CK, Tobias A, Cheng Y, Kim JW, Qiao J, Zhang L, et al. (2014). Durable therapeutic efficacy utilizing combinatorial blockade against IDO, CTLA-4, and PD-L1 in mice with brain tumors. Clin. Cancer Res 20, 5290–5301. [PubMed: 24691018]

Wang D, Green MF, McDonnell E, and Hirschey MD (2013). Oxygen flux analysis to understand the biological function of sirtuins. Methods Mol. Biol 1077, 241–258. [PubMed: 24014411]

Westendorf AM, Skibbe K, Adamczyk A, Buer J, Geffers R, Hansen W, Pastille E, and Jendrossek V (2017). Hypoxia enhances immunosuppression by inhibiting CD4+ effector T cell function and promoting Treg activity. Cell. Physiol. Biochem 41, 1271–1284. [PubMed: 28278498]

Xie J, Wang BS, Yu DH, Lu Q, Ma J, Qi H, Fang C, and Chen HZ (2011). Dichloroacetate shifts the metabolism from glycolysis to glucose oxidation and exhibits synergistic growth inhibition with cisplatin in HeLa cells. Int. J. Oncol 38, 409–417. [PubMed: 21132264]

Zagzag D, Zhong H, Scalzitti JM, Laughner E, Simons JW, and Semenza GL (2000). Expression of hypoxia-inducible factor 1alpha in brain tumors: association with angiogenesis, invasion, and progression. Cancer 88, 2606–2618. [PubMed: 10861440]

Zhang Y, Kurupati R, Liu L, Zhou XY, Zhang G, Hudaihed A, Filisio F, Giles-Davis W, Xu X, Karakousis GC, et al. (2017). Enhancing $CD8^+$ T cell fatty acid catabolism within a metabolically challenging tumor microenvironment increases the efficacy of melanoma immunotherapy. Cancer Cell 32, 377–391.e9. [PubMed: 28898698]

Zou C, Wang Y, and Shen Z (2005). 2-NBDG as a fluorescent indicator for direct glucose uptake measurement. J. Biochem. Biophys. Methods 64, 207–215. [PubMed: 16182371]

Author Manuscript Author Manuscript Author Manuscript Author Manuscript

Highlights

- HIF-1α acts as a switch to promote Treg migration at the cost of immunosuppression
- Glycolysis promotes Treg migration, while OXPHOS promotes Treg immunosuppression
- Tregs catabolize free fatty acids for immunosuppression within hypoxic brain tumors

Author Manuscript Author Manuscript Author Manuscript Author Manuscript

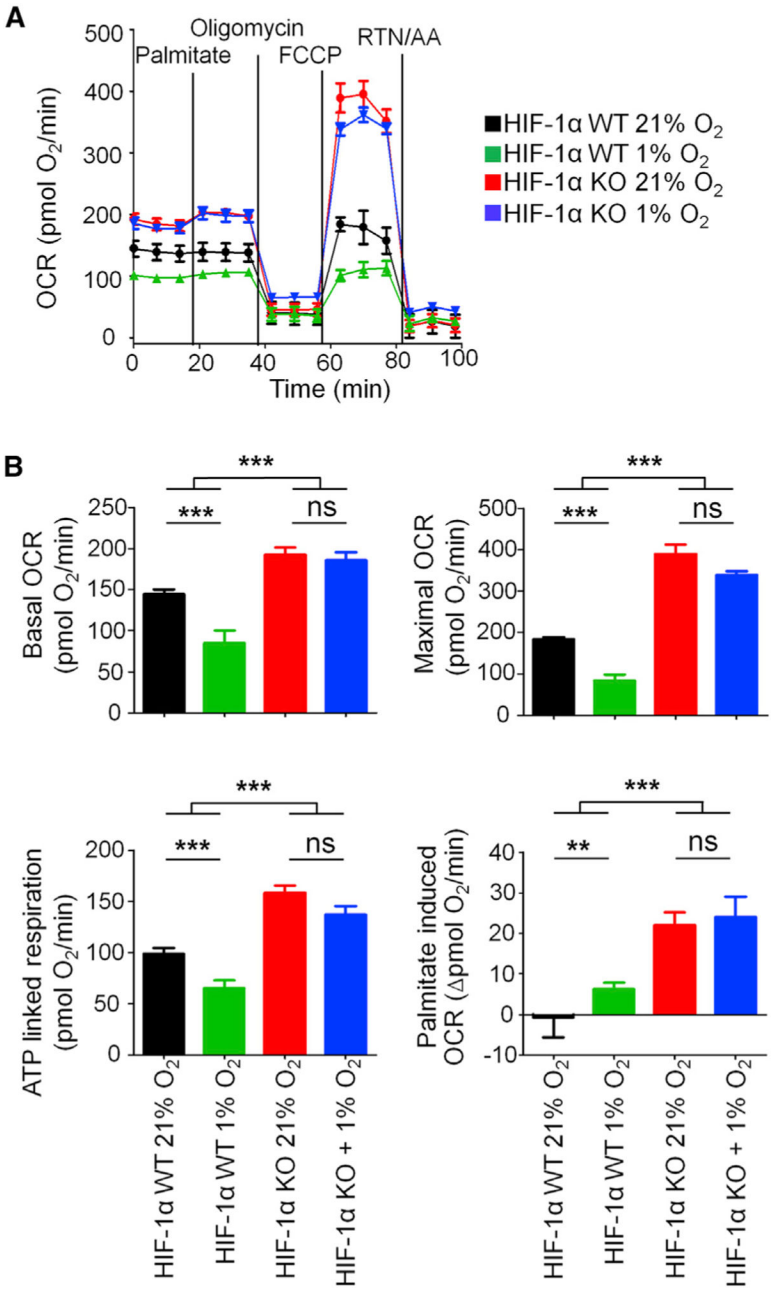

Figure 1. Deficiency of HIF-1α Promotes the Mitochondrial Utilization of Glucose under Hypoxia

(A and B) FACS-sorted and expanded Tregs from C57BL/6 Foxp3-YFP-Cre mice (HIF-1α WT) or Foxp3-YFP-Cre HIF-1α$^{flox/flox}$ mice (HIF-1α KO) were placed under normoxia or hypoxia overnight before being adhered to microplates, and oxygen consumption rate (OCR) was determined over time (A) and analyzed as bar graphs (B). A modified mitochondrial stress test was performed with an initial palmitate injection to determine palmitate-induced respiration and mitochondrial function of Tregs. Data were analyzed using Wave software from Agilent. n = 5 wells per condition were analyzed, representative of two independent experiments.

Author Manuscript Author Manuscript Author Manuscript Author Manuscript

Statistics were calculated as percent positive population ± SEM. One-way ANOVA followed by Tukey's post hoc analysis was used to calculate significance. *p < 0.05; **p < 0.01; ***p < 0.001; ns, not significant.

See also Figures S1 and S2.

Author Manuscript Author Manuscript Author Manuscript Author Manuscript

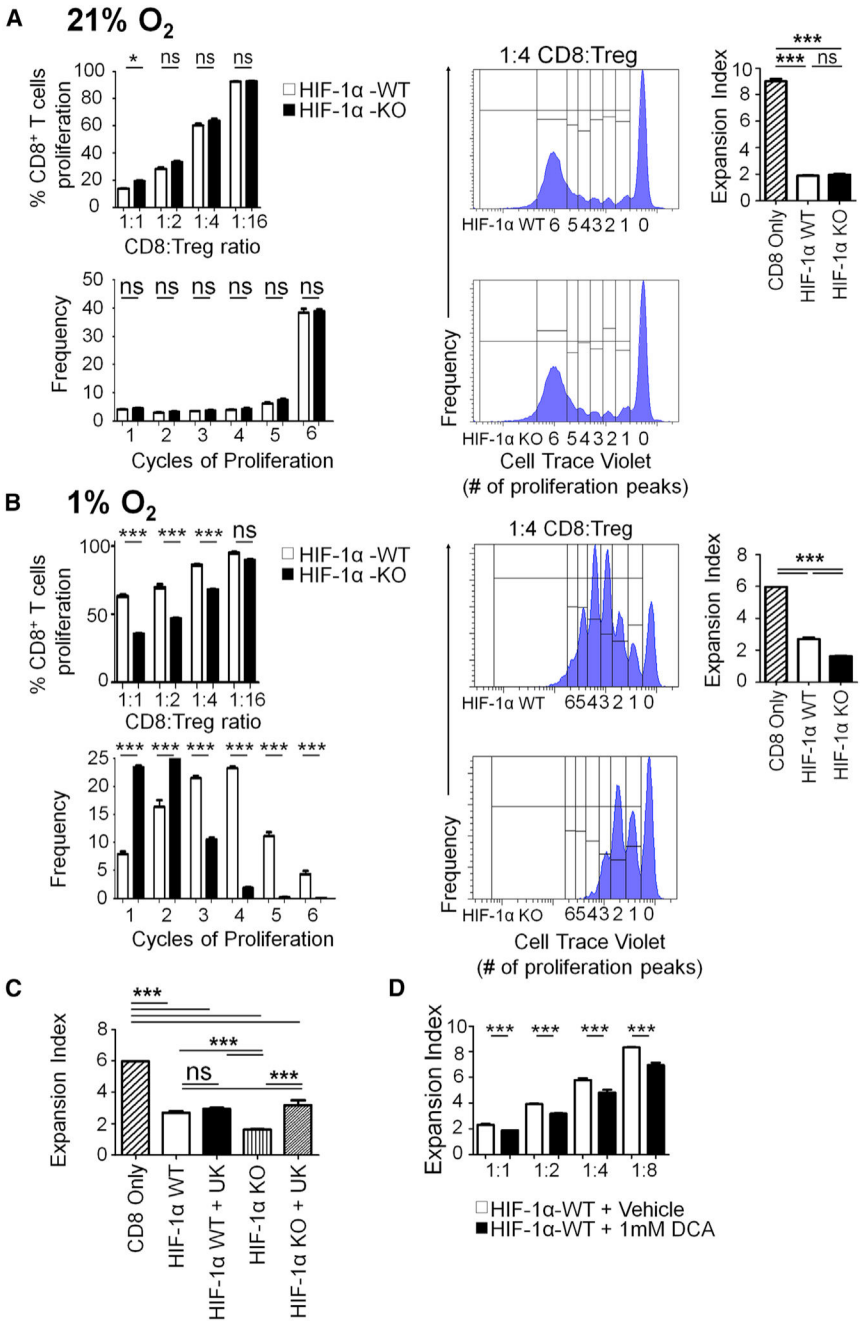

Figure 2. HIF-1α KO Tregs Suppress CD8$^+$ T Cell Proliferation Better than HIF-1α WT Tregs under Hypoxia due to Enhanced Glucose Oxidation

(A and B) Sorted and expanded Tregs were plated with proliferation-dye-labeled CD8$^+$ T cells at decreasing ratios to determine their suppressive capability under (A) 21% O_2 and (B) 1% O_2. After 72 h, CD8$^+$ T cell proliferation was analyzed. An n of 3 wells per ratio was analyzed, representative of three independent experiments.

(C) Sorted and expanded Tregs were pre-treated with UK5099 (10 μm) or vehicle control for 24 h before a suppressor assay was run under 1% O_2. After 72 h, percent proliferation and

Author Manuscript Author Manuscript Author Manuscript Author Manuscript

expansion indexes were determined via flow cytometry. An n of 3 per condition was analyzed, from two independent experiments.

(D) Sorted and expanded Tregs were pretreated with 1 mM DCA treatment overnight before suppressor assays were performed under 1% O_2.

Statistics were calculated as percent positive population ± SEM. Unpaired t test analysis was used to calculate significance. *$p < 0.05$; **$p < 0.01$; ***$p < 0.001$; ns, not significant.

Author Manuscript Author Manuscript Author Manuscript Author Manuscript

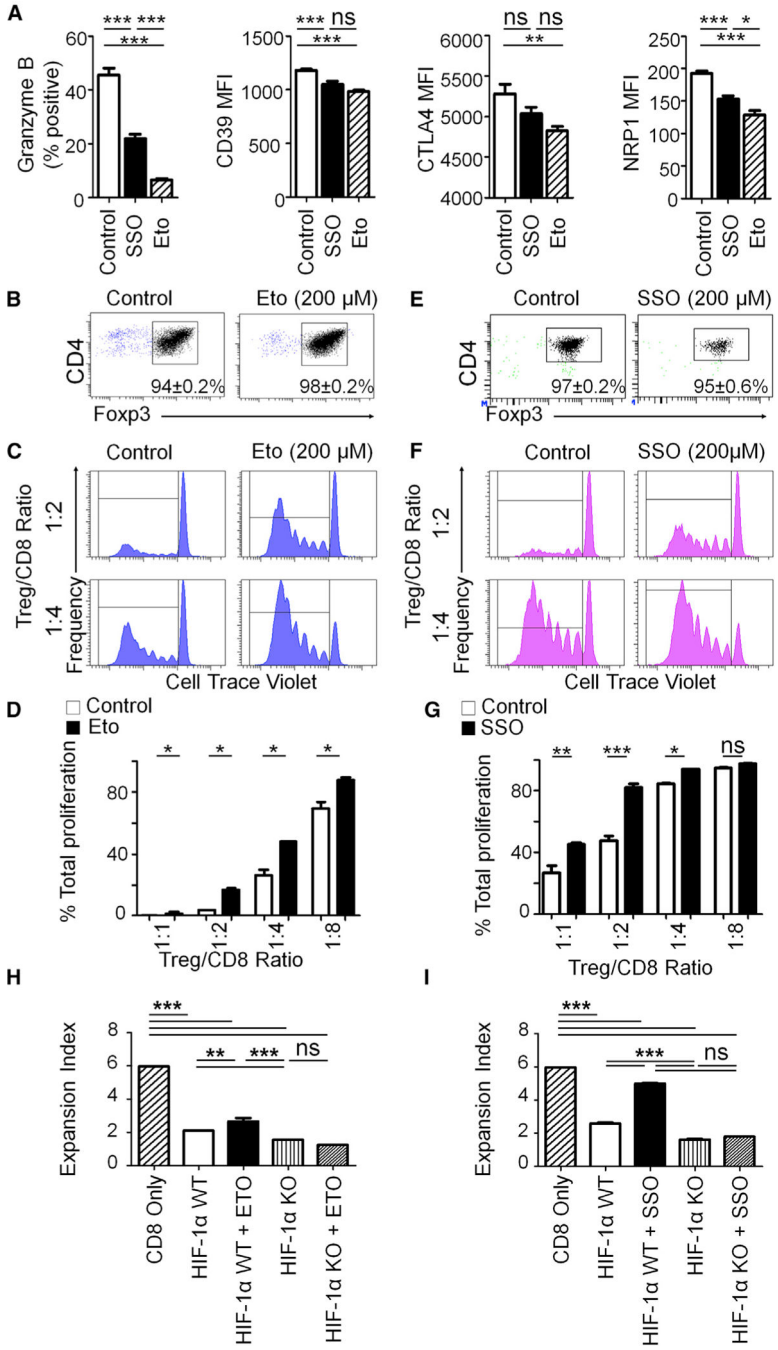

Figure 3. Inhibition of Either Lipid Uptake or Lipid Oxidation Prevents Immunosuppressive Capabilities of Regulatory T Cells

(A) Sorted and expanded Tregs were cultured for 72 h in the presence of the fatty acid oxidation inhibitor etomoxir (200 μM) or the fatty acid uptake inhibitor SSO (200 μM), and the expression of various Tregs markers was assessed via flow cytometry.

(B and E) Sorted Tregs were cultured for 72 h in the presence of etomoxir (Eto; 200 μM; B) or SSO (200 μM; E), and Foxp3 retention was determined.

Author Manuscript Author Manuscript Author Manuscript Author Manuscript

(C and D) Percent CD8 T cell proliferation with co-culture of Eto pre-treated Tregs shown as a histogram (C) and analyzed as bar graphs with reducing Treg ratios (D) that were enumerated via flow cytometry.

(F and G) Percent CD8 T cell proliferation with co-culture of SSO pre-treated Tregs shown as a histogram (F) and analyzed as bar graphs with reducing Treg ratios (G) that were enumerated via flow cytometry.

(H and I) Sorted and expanded WT or HIF-1α KO Tregs were pretreated with (H) Eto (200 μM) or (I) SSO (200 μM) for 24 h before a suppressor assay was run under 1% O_2. After 72 h, expansion indexes were determined via flow cytometry.

Flow cytometry statistics were calculated and shown as percent positive or MFI ± SEM; n = 5 per group in (A), and n = 3 per ratio in (B)–(I), representative of 2–3 independent experiments. A one-way ANOVA followed by Tukey's post hoc analysis was used to calculate significance. *$p < 0.05$; **$p < 0.01$; ***$p < 0.001$; ns, not significant.

See also Figure S3.

Author Manuscript Author Manuscript Author Manuscript Author Manuscript

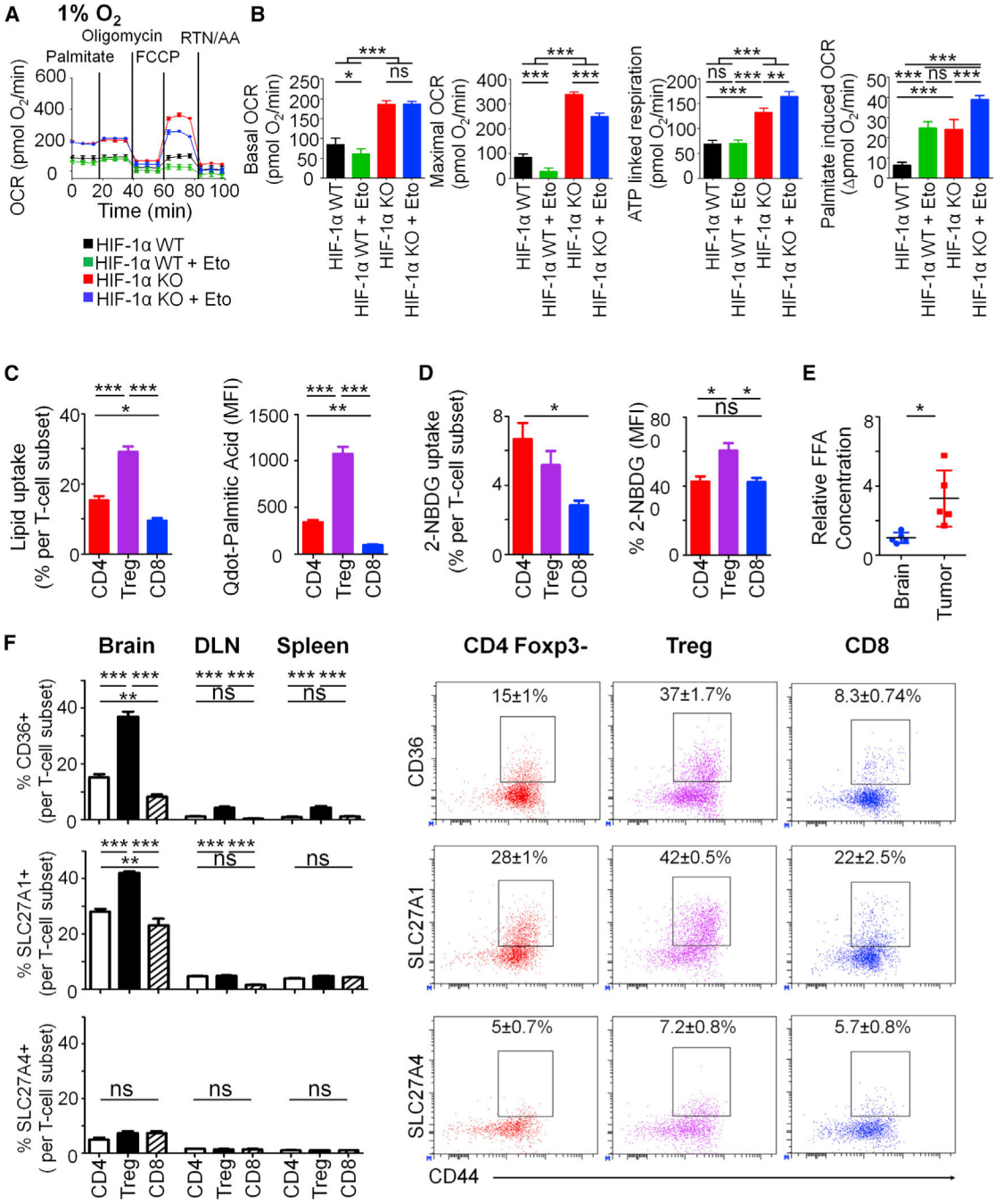

Figure 4. Regulatory T Cells Utilize Lipids for Their Mitochondrial Metabolism under Hypoxia and Prefer Lipids for Metabolism within Glioma

(A and B) Flow-cytometry-sorted and expanded HIF-1α WT or HIF-1α KO Tregs were placed under 1% O_2 overnight before being adhered to microplates, and extracellular flux analysis was performed over time (A) and analyzed as bar graphs (B). Eto treatment (20 μm) was added immediately before assay to determine reliance on lipids for mitochondrial metabolism.

Author Manuscript Author Manuscript Author Manuscript Author Manuscript

(C–F) Wild-type C57/Bl6 mice were implanted with 4×10^5 GL-261 astrocytoma cells, and after 2 weeks of tumor growth, T cell expression of surface fatty acid transporters was analyzed via flow cytometry.

(C) Percent palmitic acid uptake and MFI of conventional $CD4^+$, $CD8^+$, and Treg subsets.

(D) Percent 2-NDBG and MFI of 2-NBDG conventional $CD4^+$, $CD8^+$, and Treg subsets.

(E) Tumor interstitial fluid was obtained from either the tumor hemisphere or the non-tumor hemisphere of mice, and FFA content was measured via colorimetric readout.

(F) Data show the expression of fatty acid transporters CD36, SLC27A1, and SLC27A4 across different T cell subsets in the brains, DLN, and spleens of tumor-bearing mice (left); representative flow cytometry plots are shown on the right.

Statistics were calculated as percent positive population ± SEM. Data in (A) and (B) were analyzed using Wave software from Agilent. Statistics were calculated as percent positive population ± SEM, n = 5 per group; results are representative of three experiments in (A) and (B) and two experiments in (C)–(F). One-way ANOVA followed by Tukey's post hoc analysis was used to calculate significance. *$p < 0.05$; **$p < 0.01$; ***$p < 0.001$; ns, not significant.

See also Figure S4.

Author Manuscript Author Manuscript Author Manuscript Author Manuscript

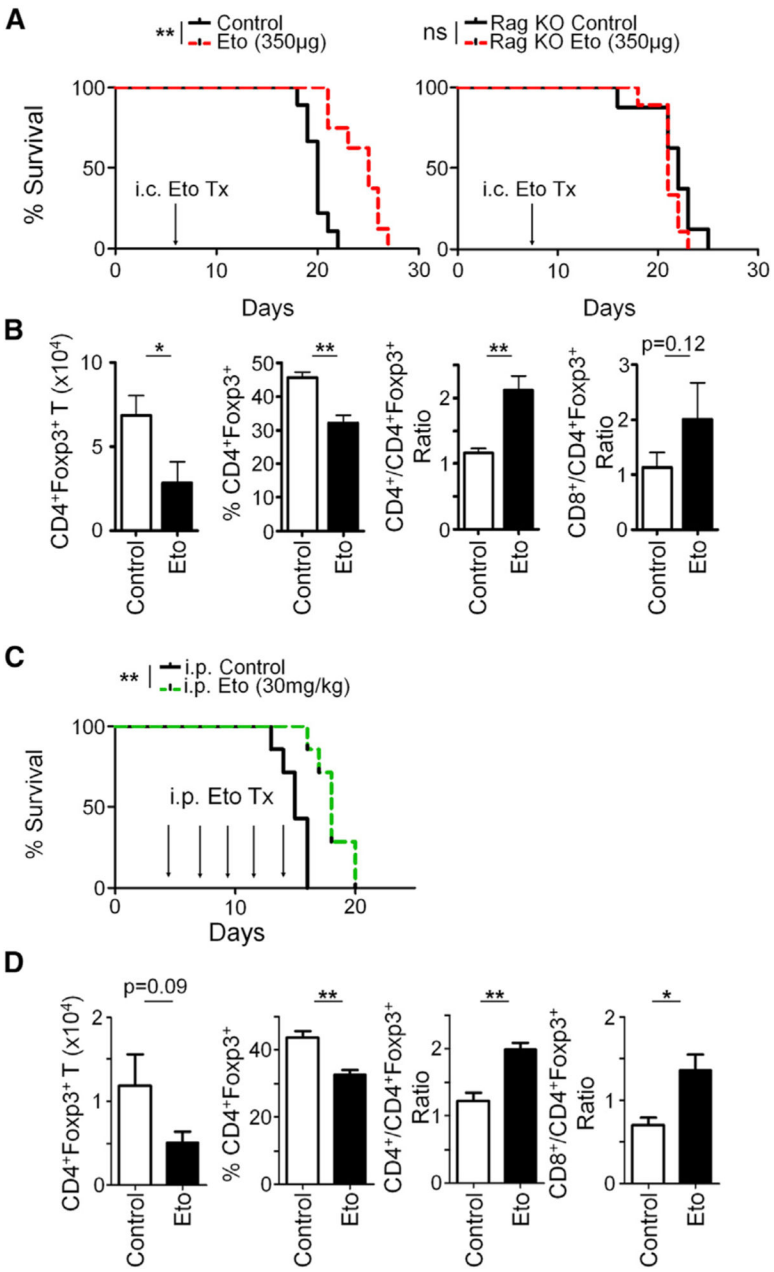

Figure 5. *In Vivo* Treatment of Eto Causes a Survival Benefit in Immunocompetent Mice

(A) Survival of WT or immunodeficient $Rag^{0/0}$ mice implanted with 4×10^5 GL-261 and treated with intracranial Eto administration beginning at day 7 after tumor implantation.

(B) Quantification of Tregs and their ratios to other T cell subsets 48 hr after Eto treatment (day 9).

(C) Survival of mice injected i.p. with 30 mg/kg Eto.

(D) Flow-cytometric analysis of Treg infiltration and their ratios to other T cell subsets 48 h after second Eto treatment (9 days). Survival curves are from at least 7 mice per group from two independent experiments; statistical significance was calculated using log-rank analysis.

Author Manuscript Author Manuscript Author Manuscript Author Manuscript

Flow cytometry statistics were calculated and are indicated as percent positive population ± SEM; n = 5 per group, representative of two independent experiments in (B) and one experiment in (D). Unpaired t test analysis was used to calculate significance. *$p < 0.05$; **$p < 0.01$; ***$p < 0.001$; ns, not significant. See also Figures S5 and S6A.

Author Manuscript Author Manuscript Author Manuscript Author Manuscript

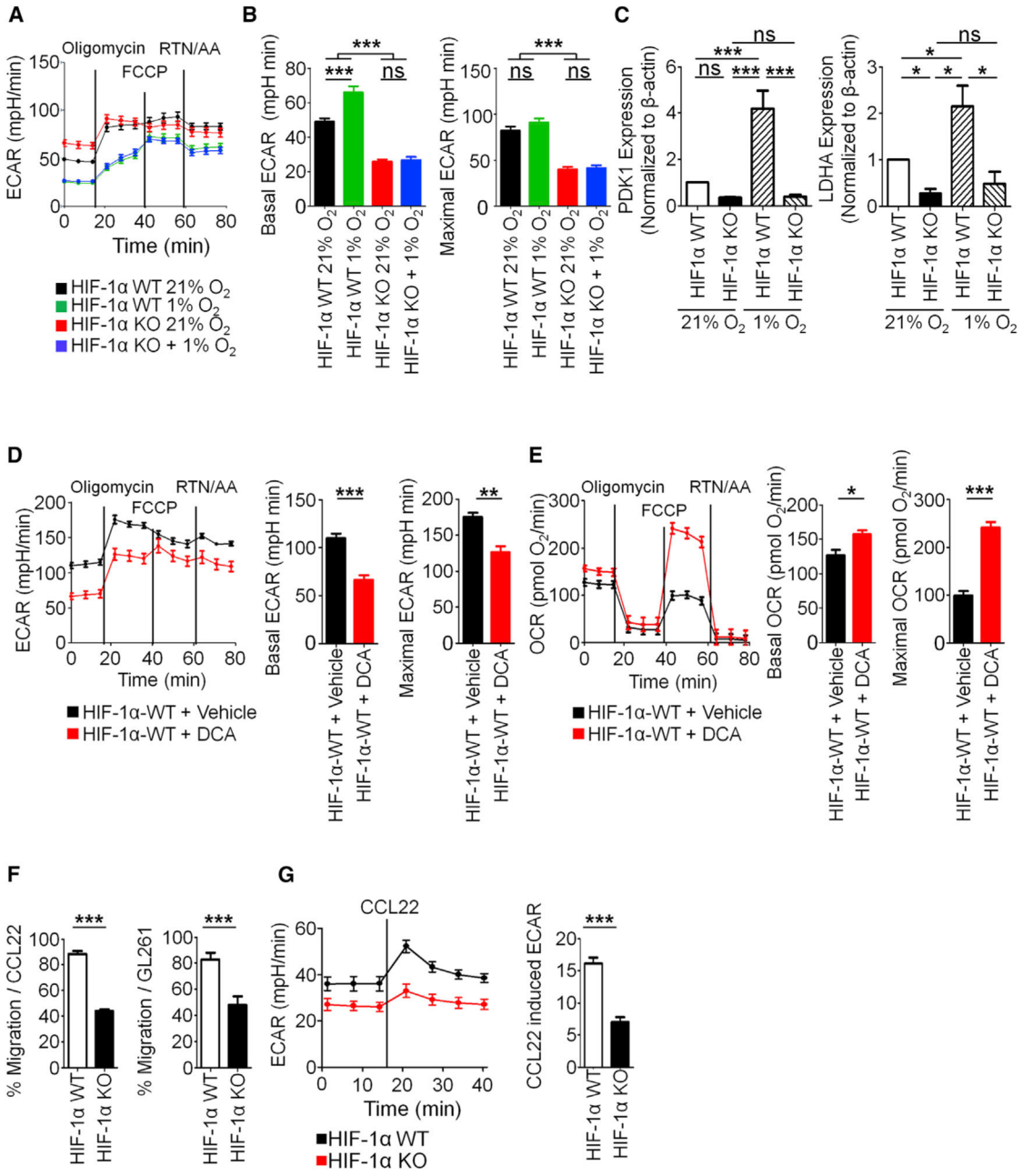

Figure 6. Deficiency of HIF-1α Inhibits Glycolytic Metabolism of Tregs, Resulting in Reduced *In Vitro* Migration

(A and B) FACS-sorted and expanded HIF-1α WT or HIF-1α KO Tregs were placed under 21% O_2 or 1% O_2 overnight before being adhered to microplates, and extracellular acidification rate (ECAR) was determined over time (A) and analyzed as bar graphs (B). (C) FACS-sorted and expanded HIF-1α WT or HIF-1α KO Tregs were put under 21% O_2 or 1% O_2 overnight, and qRT-PCR was performed to determine the expression of PDK1 and LDHA.

Author Manuscript Author Manuscript Author Manuscript Author Manuscript

(D and E) Sorted and expanded HIF-1α WT Tregs were treated with 1 mM DCA overnight before being adhered to microplates, and metabolic flux was determined over time (D) and analyzed as bar graphs (E). Data were analyzed using Wave software from Agilent.
In (A), (B), (D), and (E), an n of 5 wells per condition was analyzed, representative of two independent experiments. In (C), an n of 3 per condition was analyzed from three independent experiments.
(F) Sorted and expanded Tregs from HIF-1α WT or HIF-1α KO mice were plated in Transwell inserts to measure their migration toward the chemokine CCL22 or GL-261 tumor cells under 1% O_2.
(G) FACS-sorted and expanded HIF-1α WT or HIF-1α KO Tregs were injected with CCL22, and change in ECAR was measured.
In (F), statistics were calculated as percent migration ± SEM. In (B) and (C), one-way ANOVA followed by Tukey's post hoc analysis was used to calculate significance. In (D) and (E), unpaired t test analysis was used to calculate significance. *$p < 0.05$; **$p < 0.01$; ***$p < 0.001$; ns, not significant.
See also Figure S6B.

Author Manuscript Author Manuscript Author Manuscript Author Manuscript

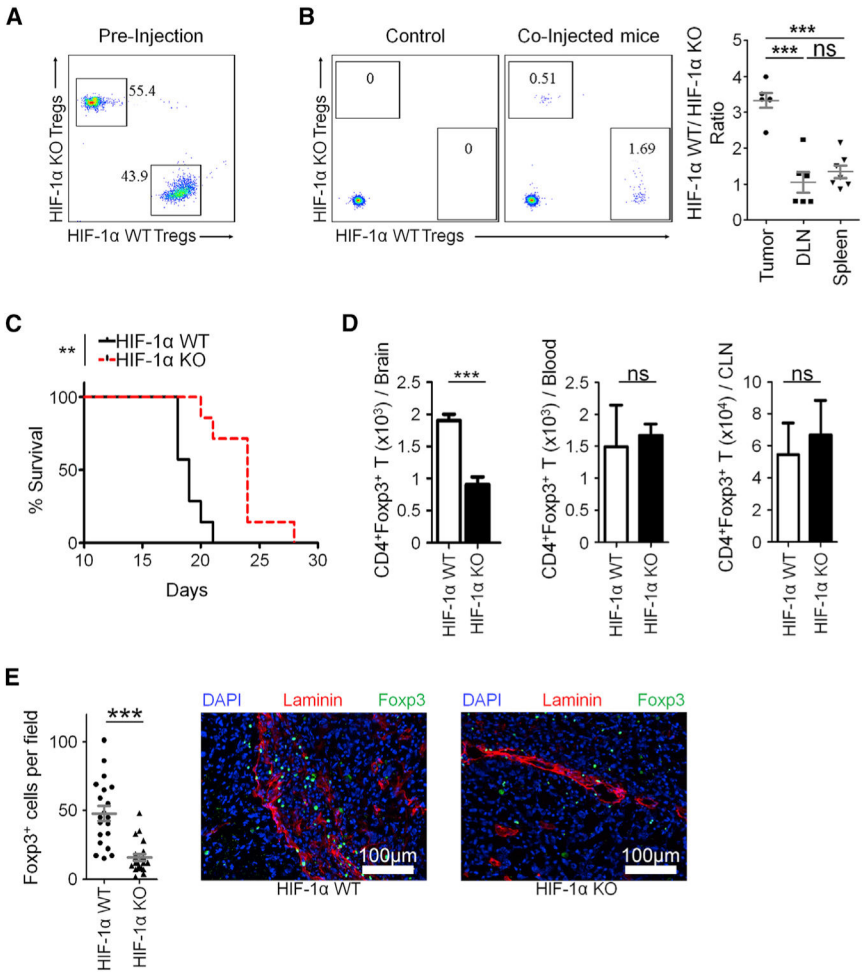

Figure 7. Conditional Knockout of HIF-1α in Foxp3$^+$ T Cells Inhibits Migration of Tregs to Brain Tumors *In Vivo*

(A) To test Treg migration *in vivo*, splenic-sorted and expanded Tregs were co-labeled with eFluor 450 (HIF-1α WT) and eFluor 670 (HIF-1α KO) cell proliferation dyes and injected i.v. at a 1:1 ratio into mice harboring GL-261.

(B) After 48 h, the brain, spleen, and DLN of mice injected with Tregs were isolated, and the ratio of control to HIF-1α KO Tregs was determined.

(C) HIF-1α WT or HIF-1α KO mice were implanted with 4×10^5 GL-261 astrocytoma cells, and overall survival was determined.

(D) After 2 weeks of tumor growth, Treg abundance was analyzed via flow cytometry.

(E) Abundance of Foxp3$^+$ cells from tumor-bearing mice was quantified in tissue sections.

Kaplan-Meier curves are n = 7 per group from two independent experiments, and significance was calculated using log-rank analysis.

Flow cytometry statistics shown as percent positive population ± SEM; n = 5 per group, representative of two experiments. In (B), the ratios of WT/HIF-1α KO Tregs were indicated as mean ± SEM. In (E), 3–5 fields per section were quantified for Foxp3$^+$DAPI$^+$ nuclei. n = 3 mice per group. Unpaired t test analysis was used to calculate significance. *p < 0.05; **p < 0.01; ***p < 0.001; ns, not significant.

Author Manuscript Author Manuscript Author Manuscript Author Manuscript

See also Figure S7.

Author Manuscript Author Manuscript Author Manuscript Author Manuscript

Cell Rep. Author manuscript; available in PMC 2019 April 12.

KEY RESOURCES TABLE

REAGENT or RESOURCE	SOURCE	IDENTIFIER
Antibodies		
Anti-CD3 Alexa Fluor 700	Biolegend	Cat#100216; RRID:AB_493697
Anti-CD3 PE-Cy7	Biolegend	Cat#100220; RRID:AB_1732057
Anti-CD4 APC	Biolegend	Cat#100516; RRID:AB_312719
Anti-CD4 Biotin	Biolegend	Cat#100508; RRID:AB_312711
Anti-CD4 Percp-Cy5.5	Biolegend	Cat#100540; RRID:AB_893326
Anti-CD4 PE-Cy7	Biolegend	Cat#100528; RRID:AB_312729
Anti-CD4 Pacific blue	Biolegend	Cat#100531; RRID:AB_493374
Anti-CD45 PE	Biolegend	Cat#103106; RRID:AB_312971
Anti-CD8 Biotin	Biolegend	Cat#100714; RRID:AB_312753
Anti-CD8 APC	Biolegend	Cat#100712; RRID:AB_312751
Anti-CD8 BV605	Biolegend	Cat#100744; RRID:AB_2562609
Anti-CD44 PE	Biolegend	Cat#103008; RRID:AB_312959
Anti-CD25 Alexa 700	Biolegend	Cat#102024; RRID:AB_493709
Anti-CD36 APC	Biolegend	Cat#102611; RRID:AB_571994
Anti-CTLA4 PE	Biolegend	Cat#106306; RRID:AB_313255
Anti-Granzyme B Alexa 647	Biolegend	Cat#515406; RRID:AB_2566333
Anti-NRP1 PE-Cy7	Biolegend	Cat#145211; RRID:AB_2562359
Anti-CD39 Alexa 647	Biolegend	Cat#143807; RRID:AB_2563977
Anti-SLC27A1	Sigma	Cat#SAB1402095; RRID:AB_10609989
Anti-SLC27A4	Abeam	Cat#ab200353; RRID:AB_2716563
Anti-Foxp3 EFIuor 450	Fisher	Cat#48–5773–82; RRID:AB_1518812
Anti-Foxp3 Biotin	Fisher	Cat#13–5773–82; RRID:AB_763540
Goat anti rabbit Alexa 647	Fisher	Cat#A-21236; RRID:AB_141725
Streptavidin Alexa 488	Jackson Immunoresearch	Cat#016–540–084; RRID:AB_2337249
Anti-Laminin Alexa 647	Novus	Cat#NB300–144AF647
Bacterial and Virus Strains		
Biological Samples		N/A
Chemicals, Peptides, and Recombinant Proteins		

Author Manuscript Author Manuscript Author Manuscript Author Manuscript

REAGENT or RESOURCE	SOURCE	IDENTIFIER
Sulfo-N-suooinimidyl Oleate	Cayman	Cat#11211
Etomoxir Sodium Salt	MedChem Express	Cat#HY-50202A
Palmitate-BSA	Agilent	Cat#102720–100
Sodium Dichloroacetate	Sigma	Cat#347795
Cell Trace Violet	Fisher	Cat#C34557
Fluoroshield with DAPI	Sigma	Cat#F6057–20ML
UK5099	Cayman	Cat#16980
Quantum Dot 605 - Palmitate conjugate	In lab	N/A
Dynabeads T cell Expander	Fisher	Cat#11452D
Recombinant IL-2	Peprotech	Cat#212–12
Recombinant TGF-β	Peprotech	Cat#100–21
Recombinant CCL22	Peprotech	Cat#250–23
2-NBDG	Fisher	Cat#N13195
Cell Proliferation Dye eFluor 450	Fisher	Cat#65–0842–90
Cell Proliferation Dye eFluor 670	Fisher	Cat#65–0840–85
Cel Tak	Fisher	Cat#CB-40240
Critical Commercial Assays		
MitoStress Test	Agilent	Cat#103015–100
Xfe96 Flux Paks	Agilent	Cat#102416–100
Murine T cell Magnisort Enrichment kit	Fisher	Cat#8804–6820–74
Deposited Data		
Raw and Analyzed data	Mendeley	https://data.mendeley.com/datasets/k8z9vbmddc/1
Experimental Models: Cell Lines		
Murine glioma GL-261 Sex: M	NCI	DTP, DCTD TUMOR REPOSITORY RRID:CVCL_Y003
GBM6 Age/Sex:65/M	C. David James, Northwestern University	N/A
GBM12 Age/Sex:68/M	C. David James, Northwestern University	N/A
MES83 Age/Sex: Unknown/F	from Ichiro Nakano, University of Alabama at Birmingham and Shi-Yuan Cheng, Northwestern University	N/A
Experimental Models: Organisms/Strains		
MOUSE: C57 BI/6	Jackson	Cat#000664; RRID:IMSR_JAX:000664
MOUSE: Foxp3-$^{YFP–CRE}$	Jackson	Cat#016959; RRID:IMSR_JAX:016959

Author Manuscript Author Manuscript Author Manuscript Author Manuscript

REAGENT or RESOURCE	SOURCE	IDENTIFIER
MOUSE: Foxp3-Hif1a-$^{fl/fl}$	Jackson	Cat#007561; RRID:IMSR_JAX:007561
MOUSE: Foxp3-$^{YFP–CRE}$ × Hif1a-$^{fl/fl}$	This Paper	N/A
MOUSE: Rag1$^{0/0}$	Jackson	Cat#002216; RRID:IMSR_JAX:002216
Oligonuoleotides		
β-Actin Forward: TTGCTGACAGGATG CAGAAG	Purchased: IDT	Design: ncbi.nlm.nih.gov/tools/primer-blast/
β-Actin Reverse: ACATCTGCTGGAAG GTGGAC	Purchased: IDT	Design: ncbi.nlm.nih.gov/tools/primer-blast/
PDK1 Forward: GGACTTCGGGTCAGT GAATGC	Purchased: IDT	https://pga.mgh.harvard.edu PrimerBank ID: 27369966a1
PDK1 Reverse: TCCTGAGAAGATTGT CGGGGA	Purchased: IDT	https://pga.mgh.harvard.edu PrimerBank ID: 27369966a1
LDHA Forward: TGTCTCCAGCAAAGA CTACTGT	Purchased: IDT	https://pga.mgh.harvard.edu PrimerBank ID: 6754524a1
LDHA Reverse: GACTGTACTTGACAAT GTTGGGA	Purchased: IDT	https://pga.mgh.harvard.edu PrimerBank ID: 6754524a1
Software and Algorithms		
Prism	Graphpad	www.graphpad.com; RRID:SCR_002798
Facs Diva	BD	www.bdbiosciences.com
Excel	Microsoft	www.microsoft.com; RRID:SCR_016137
FlowJo	Treestar	www.flowjo.com; RRID:SCR_008520
Wave	Agilent	www.agilent.com; RRID:SCR_014526
ImageJ	NIH	imagej.nih.gov/ij/; RRID:SCR_003070